METAL ORGANIC FRAMEWORKS WITH SPECIAL TOPOLOGY AND OPEN METAL SITES FOR IMPROVED HYDROGEN ADSORPTION

A Thesis

by

MELIH BACI

Submitted to the Office of Graduate and Professional Studies of
Texas A&M University
in partial fulfillment of the requirements for the degree of

MASTER OF SCIENCE

Chair of Committee,	Hong-Cai Joe Zhou
Committee Members,	David Barondeau
	Tahir Cagin
Head of Department,	Simon North

August 2019

Major Subject: Chemistry

Copyright 2019 Melih Baci

ABSTRACT

Hydrogen is a promising candidate as a replacement of fossil fuels due to its zero-carbon emission upon combustion. Storage of hydrogen is one of the most important technical challenges especially for on-board applications because of its low density. Along with many other candidates such as chemical storage materials like hybrid metal hydrides and physical storage candidates like zeolites, hydrogen storage in metal organic frameworks (MOFs) has been studied extensively for the last two decades for their high potential to be used in on-board storage applications.

One of the promising MOF materials is PCN-12 due to having open copper sites which enhances interactions with the hydrogen and its unique topology which maximizes the interactions further. Although PCN-12 shows great potential, it has not received enough attention mainly due to technical challenges during its synthesis which would require usage of sealed pyrex tubes and gradual temperature changes over a day.

In this study, we have demonstrated a facile solvothermal synthesis method for PCN-12 with high yield (79% based on ligand) and high crystallinity by adding an optimized amount of nitric acid to the solution of the ligand and metal salt. We have also investigated the effect of nitric acid amount on crystal formation and adsorptive properties of PCN-12. Furthermore, we have attempted to synthesize new MOF structures based on PCN-12 in order to investigate their hydrogen storage properties.

DEDICATION

To Dr. Hongcai Joe Zhou and Dr. Omer Dag,

For their support and encouragement through years

ACKNOWLEDGEMENTS

I would like to thank my advisor Dr. Hong-Cai Zhou for providing me excellent opportunities to conduct research and develop researcher skills during my studies. I also thank my committee members Dr. David Barondeau and Dr. Tahir Çağın for their support and helpful advices.

I would like to thank past and present Zhou group members whom I have learned a lot on multiple occasions, especially to Dr. Kecheng (Kevin) Wang for useful discussions and Dr. Jiandong Pang for useful discussions and teaching me high pressure data analysis, to Sayan Banerjee and Angelo Kirchon for their contributions and discussions, to Gregory Day, Zachery Perry, Dr. Shuai Yuan and many others for their encouragement, helpfulness and being amazing colleagues. I also thank Rahym Ashirov for proofreading and suggesting edits to clarify its language.

Lastly but the most importantly, I am very thankful to my parents, Suat Sami and Hamiyet, and to my siblings, Muhittin, Hilal and Zeynep for their endless support and providing me a very happy and a warm family environment, the reason of any success I would achieve in my life.

CONTRIBUTORS AND FUNDING SOURCES

Contributors

This work was supervised by a thesis committee consisting of Professor Dr. Hong-Cai Zhou [advisor] and Professor Dr. David Barondeau of the Department of Chemistry and Professor Dr. Tahir Çağın of the Department of Material Science and Engineering.

The high-pressure adsorption data analyzed for Chapter III was provided by Sayan Banerjee.

All other work conducted for the thesis was completed by the student independently.

Funding Sources

Graduate study was supported by a fellowship from Texas A&M University.

NOMENCLATURE

BET	Brunauer-Emmett-Teller
CGH_2	Compressed Hydrogen Gas
CCDC	The Cambridge Crystallographic Data Centre
CSD	Cambridge Structural Database
DMA	*N*,*N*-Dimethyl Acetamide
DMF	*N*,*N*-Dimethyl Formamide
DMSO	Dimethyl Sulfoxide
DOE	United States Department of Energy
HKUST	The Hong Kong University of Science and Technology
LH_2	Liquid Hydrogen
MeOH	Methanol
MOF	Metal-Organic Framework
NMR	Nuclear Magnetic Resonance
PCN	Porous Coordination Network
PXRD	Powder X-Ray Diffraction
Q_{st}	Isosteric Heat of Adsorption
SBU	Secondary Building Unit
SSA	Specific Surface Area
STP	Standard Temperature & Pressure
TGA	Thermogravimetric Analysis

TABLE OF CONTENTS

Page

LIST OF FIGURES

Page

LIST OF TABLES

Page

LIST OF SCHEMES

Page

CHAPTER I

INTRODUCTION

1.1. Hydrogen Storage

The search to find alternative fuels to the current carbon emitting sources like gasoline has been receiving increasing attention due to recent climate change reports and to prevent a potential crisis for there are limited resources of carbon-based fuels. Hydrogen is considered one of the promising alternatives for two important reasons: one being a zero-carbon emission fuel as its sole product after combustion is water and the second is its higher gravimetric energy density, tripling the density of gasoline.[1] Although hydrogen is not considered to be an energy source and needs to be produced in order to be used, it is fairly abundant in other forms such as in water so can be generated from other energy sources. Along with a need to develop technologies to generate it, storage of hydrogen is also a key challenge for hydrogen to be a successful alternative, especially where mobility is required such as in the case of transportation.

Various methods and their operating conditions have been reported as potential hydrogen carriers (Figure 1). Unfortunately, none of these candidates meet the requirements yet to be an ideal method, particularly, cost effective, practical or safe. Being one of the most matured systems, most prototypes are using the compressed hydrogen gas (CGH_2) method due to its practical operating conditions, however, high pressure (around 70 MPa) introduces technical challenges in terms of safety. The liquid hydrogen (LH_2) method could help overcome the high pressure related challenges, however, it suffers from

even harder challenges since the operating temperature needs to be below -253 °C otherwise hydrogen would evaporate. Because of the limitations of these two basic systems, chemical and physical storage materials are attracting researchers from material sciences and chemistry fields. Most chemical storage materials are composed of main group metal hydrides and some include hybrid hydrides of transition metals. These structures have great potential for on-board applications because of their high densities. Strong binding of hydrogen atoms (also involves splitting of H-H bond) allows them to overcome high-pressure requirements and can store hydrogen at a density even higher than LH_2. One of the greatest challenges of researching these materials is achieving reversible decomposition of the hydrogen.[2] They mostly require a chemical off-board regeneration process and reusability is often limited because of the chemical degradation after each hydrogenation-dehydrogenation cycle. Physisorption materials such as activated carbon, zeolites and MOFs on the other hand, can easily be recharged with hydrogen as there is no structural change observed upon adsorption-desorption process. These systems mostly suffer from low adsorption amounts at ambient temperature simply because of weak Van der Waals interactions between the sorbent and hydrogen. For zeolites and carbon-based structures, it is shown that the adsorbed amount is correlated with the specific surface area (SSA) of the material, so their storage performances are limited by the surface area.[3] The empirical law of this correlation is often called Chahine's Rule and will be discussed in detail later. Although carbon-based structures like activated carbons and nanotubes have received great attention, zeolites have not been studied extensively due to their limited surface areas.

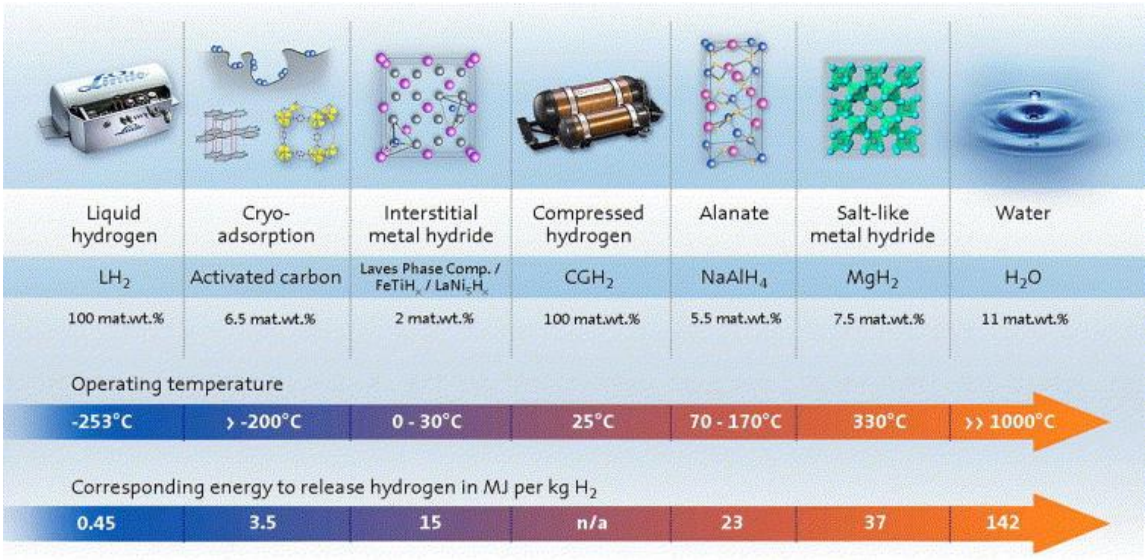

Figure 1. Different hydrogen technologies and their working conditions. (Reprinted with permission from Ref [4], copyright © 2007 Elsevier, Inc.)

1.2. Metal-Organic Frameworks

Metal-organic frameworks (MOFs) are a class of crystalline coordination compounds made of mostly organic compounds with multiple binding units called linkers and metal ions or clusters called secondary building units (SBUs). Their defined structure made of repeating units, permanent porosity and extreme tunability by employing various metal substructures and almost infinitely different linker possibilities make them ideal structures to study for various reasons, therefore, have been attracting increasingly number of researchers ever since they have been discovered.

Porous materials include carbon-based structures like activated carbon, silica and alumina-based structures like zeolites, porous polymers and MOFs. Because of their synthesis procedures, most porous materials have some level of randomness in their pore

size distributions they inherit during the process of structure formation therefore some random inaccessible space in their structures. Among the porous structures, MOFs have the most significant advantages of having well defined crystalline structures allowing them to have certain size and shape of pores. Being able to utilize majority of the molecular surface of the linkers, all except the surface connecting the metal nodes, MOFs are among the record high specific surface are materials with examples exceeding 7000 m^2/g.[5] Most MOFs have micropores (pore diameter smaller than 2 nm), as their pores are mostly defined by the size of the linkers and the topology, however, there are increasing number of mesoporous examples (mesopores have a diameter of 2 nm to 50 nm) and various methods to form mesopores in their structures.

Discovery of MOF-5 was a big breakthrough for the research of porous materials as it had significantly higher surface area than commonly studied zeolites of the time, and since then, extensive research has been done on MOFs. Due to their highly tunable structures; extraordinary properties such as extreme thermal and chemical stabilities, conductivity, luminescence, high surface areas and ultra-high amounts of adsorption of specific molecules have been explored. Furthermore, MOFs have been successfully employed in applications such as various heterogenous catalysis, sensing, gas storage and

separation. This work will be focused more on hydrogen gas adsorption in MOFs, specifically in the best performing structures.

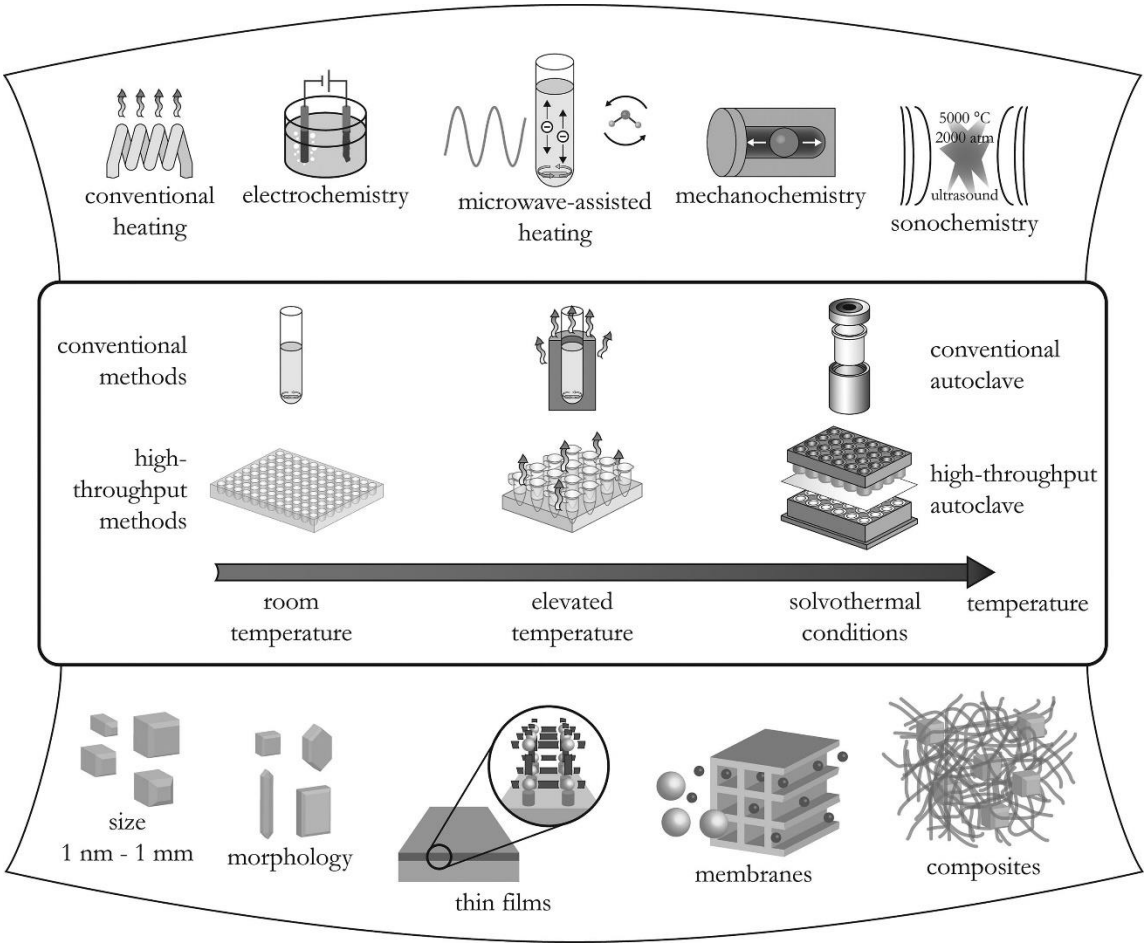

Figure 2. Synthesis methods and possible products of MOFs. (Reprinted with permission from Ref [6], copyright © 2012 American Chemical Society)

Synthesis of MOFs are usually done through solvothermal methods, mostly in polar and even protic solvents (Figure 2). Conditions like temperature, concentrations of the metal salt and the ligand, pH and the nature of the solvent may have great impact on the crystal morphology. Considering that there is still some mystery to a simple

phenomenon like solubility, growth of MOF crystals has a certain degree of chaotic nature. Therefore, study of MOF crystal growth relies heavily on screening studies. Luckily, kinetics and thermodynamics of the crystal growth are heavily studied and methods to simplify screening studies are established such as kinetically tuned dimensional augmentation (KTDA).[7] This method allows to grow large single crystals of various linkers and μ_3-oxo cluster by utilizing a tuned amount of another carboxylate source called the modulating reagent. Generally, the parameters of these screening studies involve usage of different temperatures, solvent systems, concentrations of the reagents and modulating reagents.

1.2.1. Hydrogen Storage in Metal-Organic Frameworks

MOFs are classified as physisorption materials which store hydrogen reversibly adsorbed on the surface. Like other physisorption material such as zeolites and activated carbon, ideal operating temperatures are far below the room temperature, due to weak interactions mentioned earlier. However, unlike aforementioned materials, MOFs can have significantly higher specific surface areas and their extreme tunability make them attractive candidates to overcome the barriers other physisorption materials face. Examples of MOFs have exceeded 9.9 weight % excess hydrogen adsorption at 77 K and under 100 bar pressure.[8] Even though these results are remarkable, achieving similar results at ambient temperature still remains a challenge as adsorbed amounts drop below 1% (roughly below 10% of the adsorbed amount at 77 K).

Handling of the material and experimental details may also have huge impact on the performance as well. Because of having different crystallinity of the prepared sample and activation conditions, varying hydrogen adsorption data between 1.3 and 7.1 wt.% maximum excess uptake at 77 K were reported.[9]

1.2.1.1. Analysis of MOFs for Hydrogen Storage

Crystallography and gas sorption studies are the pillars of structural analysis of MOFs due to their crystalline structures and porosity. While spatial arrangement of atoms is uncovered by x-ray diffraction (XRD) studies; surface area, pore size and distribution, and the uptake amount of specific gases can be obtained by using surface area analysis methods. With these studies, parameters like adsorption capacity and adsorption enthalpy can be obtained which are very helpful to determine the hydrogen storage performance of these materials.

1.2.1.1.1. Excess and Total Uptake

Hydrogen stored within the pores of the MOF crystals can be found either as adsorbed or floating in the void space. The adsorbed amount is approximated by the pore analysis measurement, measured as excess uptake. Excess uptake is measured as the extra amount of hydrogen contained in presence of the adsorbent subtracted by the amount that would occupy the same volume in absence of the adsorbent. Total uptake, which is the total amount of hydrogen found within the pores is calculated as the sum of the measured excess uptake and a calculated amount of gaseous hydrogen in the pore space of the MOF,

also represented in Figure 3.[10] To calculate the free gas amount, experimentally obtained pore volume is multiplied by the density of the hydrogen at given temperature and pressure, which yields the following equation:

$$n_{tot} = n_{ex} + \rho_{bulk}\,(P, T) \qquad (1)$$

The pore volume is calculated by subtracting the skeletal volume of the crystal by bulk volume. The bulk volume is calculated using the crystallographic parameters and the skeletal volume is determined by helium expansion experiment. Although the absolute uptake, the total amount adsorbed by the MOF is what is sought after; it cannot be directly calculated as it is difficult to determine the size of the adsorbed space experimentally. Therefore, researchers mostly report both experimentally obtained excess uptake, as well as the calculated total uptake as an estimation of the absolute uptake. Under low pressure regime (lower than 1 atm), the total and the excess uptake values are nearly identical due to low density of hydrogen in the gaseous phase. However, significant deviation of the excess and total uptake is observed under higher pressure regime (10 – 100 atm) due to compression of the gaseous form of hydrogen.

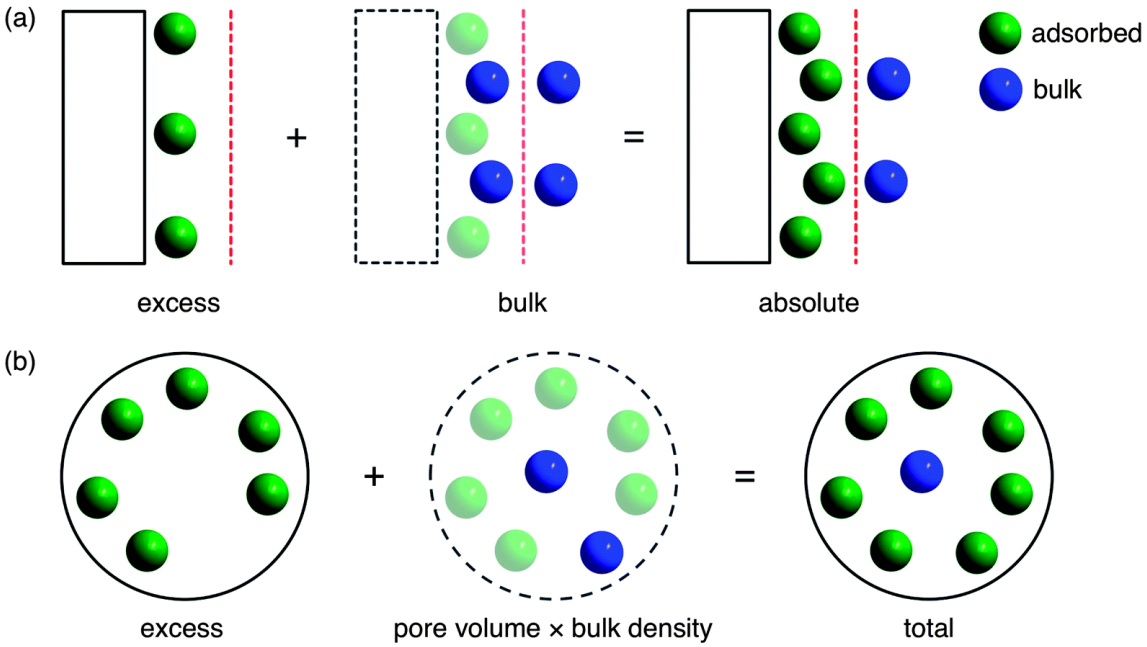

Figure 3. Representation of excess and absolute (total) uptake. The red line refers to Gibbs dividing surface, green spheres refer to adsorbed gas on the surface, while blue spheres refer to non-adsorbed (bulk) gas within the pores. Pore volume and excess uptake are experimentally determined, and the total uptake is calculated as an estimation of the absolute uptake using the density of the gas, pore volume and the excess uptake. (Reprinted with permission from Ref. [11], copyright © 2014 The Royal Society of Chemistry)

1.2.1.1.2. Chanine's Rule

Named after Dr. Richard Chahine, the rule is an empirical relation observed on porous carbon structures which estimates about 1 wt.% of hydrogen adsorption per 500 m^2/g specific surface area. It can be obtained by assuming all the accessible surface of any given carbon structure is composed of sp^2 hybridized hexagonal lattice and one hydrogen molecule is adsorbed on each adjacent hexagon (Figure 4). Using the theoretical specific surface area of graphene sheet (2630 m^2/g) and the calculated % weight of adsorbed

hydrogen on graphene (5.6 wt.%), 1.06 wt.% of hydrogen per 500 m^2/g surface area rule can be deduced.

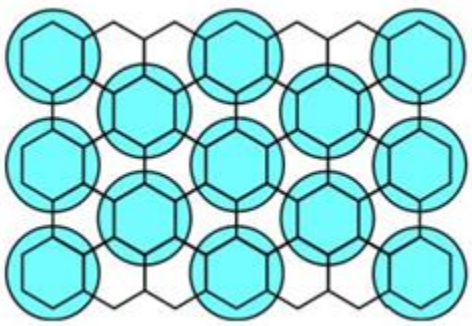

Figure 4. Close packing of hydrogen molecules on hexagonal lattice of sp^2 carbon. Having one hydrogen on each blue sphere on both sides of the surface leads to 5.6 wt.% hydrogen adsorption on carbon.

This rule was reported to hold true for variety of carbon structures synthesized by different methods including different types of activated carbon and single walled carbon nanotubes with a fair margin of error (Figure 5).

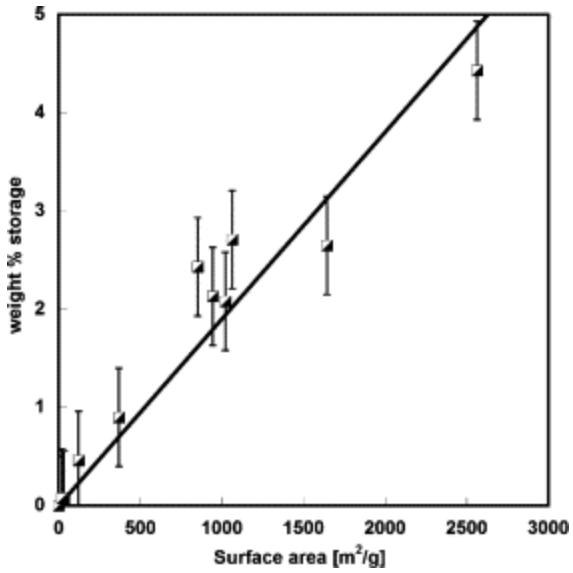

Figure 5. Hydrogen storage capacity of carbon structures and their specific surface areas at 77 K. The slope is reported as $1.91 \cdot 10^{-3}$ wt.% g m^{-2}, which is very close to theoretical estimation of $2.11 \cdot 10^{-3}$ wt.% g m^{-2}. (Reprinted with permission from Ref.[12] copyright © 2005 Elsevier, Inc.)

At high pressure like carbon structures tested, MOFs follow a similar trend with many examples surpassing the rule. A similar trend with a lower slope is also observed at low pressure regime, however, the behavior changes beyond 2000 m^2/g SSA and gravimetric hydrogen uptake does not benefit from extra surface area.

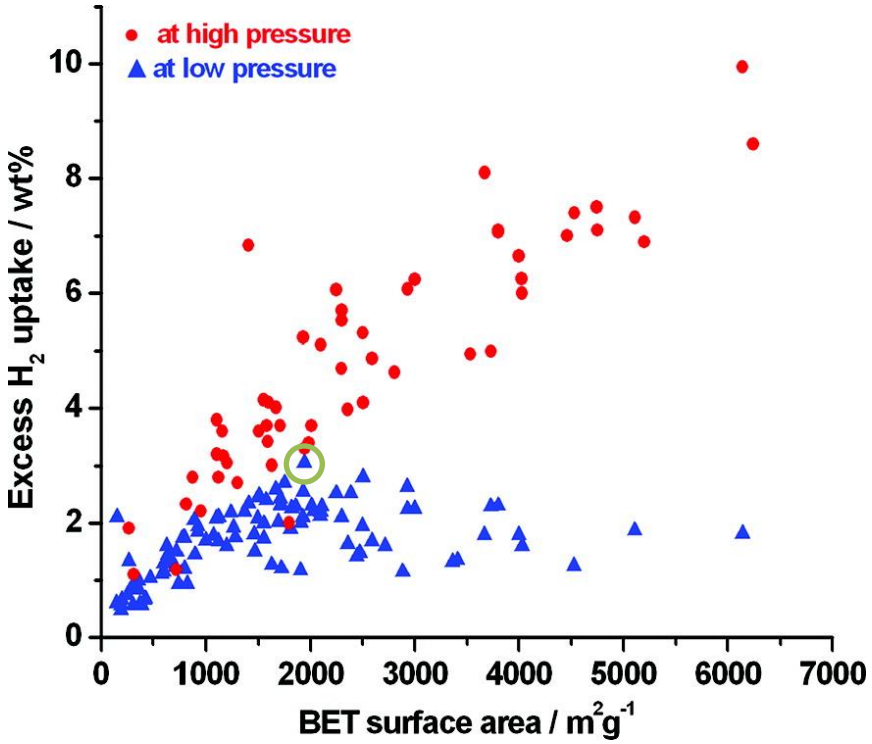

Figure 6. Hydrogen uptake capacities of various MOFs at 77 K with respect to their BET surface areas. Low pressure refers to 1 atm and high pressure is from 10 atm to 90 atm. PCN-12 is found at near 2000 m^2/g and 3.0 wt% (circled), being the highest reported at low pressure regime. (Reprinted with permission from Ref. [13], copyright © 2012 American Chemical Society)

Surpassing Chahine's rule is correlated to achieving stronger surface-hydrogen interactions by manipulating the MOF surface. Many reported MOFs which achieve higher surpassing have SBUs with open metal sites, which is a term used for uncoordinated metals within the MOF crystals (Figure 6). The open metal sites help perturb the pore space by polarizing the binding hydrogen and therefore additional hydrogen molecules can be adsorbed on the surface with stronger surface interactions. A measure of how much they surpass can be calculated using the following formula, as per Chahine's rule, expected adsorption is 1 wt.% per 500 m^2/g:

$$over\ Chahine's\ rule = \frac{excess\ uptake\ (wt.\%)\ -\ BET\ SSA\ (m^2/g)/500}{BET\ SSA\ (m^2/g)/500} \quad (2)$$

MOFs with open metal sites, especially with di-copper paddlewheel SBUs could have significantly high surpassing ratios. Among the best examples, higher surpassing is usually observed with lower surface area MOFs, although not perfectly correlated. It could be related to the open metal sites, as the higher surpassing observed with lower SSA MOFs diminish with higher SSA MOFs like in the examples of MOF-210 and NU-100, where negative numbers are obtained. This trend can be attributed to decreasing open metal site density as the surface area increases, as the effect of the open metal site to the adsorption would lessen.

Table 1. Examples of MOFs with different Chahine's rule surpassing ratios

MOF Name	% Over Chahine's rule	BET Surface Area (m^2/g)	Gravimetric Excess Uptake (wt.%)	Ref.
PCN-11	35.0	1931	5.23	[14]
NOTT-101	34.8	2247	6.06	[15]
PCN-12*	29.5	2285	5.92	*this work
PCN-14	26.1	1753	4.42	[16]
NU-100	-19.0	6143	9.95	[8]
MOF-210	-31.1	6240	8.60	[5]

1.2.1.1.3. Gravimetric and Volumetric Adsorption Capacities

Increasing both gravimetric and volumetric hydrogen uptake are major concerns for hydrogen storage research of physisorption materials research. The U.S. Department of Energy (DOE) had 2017 targets set at 5.5 wt.% gravimetric and 40 g/L volumetric storage capacity. At 77 K, majority of MOFs are reported to follow a trend where both capacities increase linearly first, and then the volumetric capacity slopes down as gravimetric capacity further increases (Figure 7). This trend can be explained by the relation of specific surface area and MOF density. Gravimetric capacity is mostly correlated to the specific surface area for the MOFs with large surface areas as Chahine's rule states, and the MOF density reduces as the surface area increases because increase in void space within the MOF crystal. This phenomenon shows the importance of volumetric uptake when on-board applications is the main concern, as when MOFs with ultra-large surface areas are used, the tank to store the hydrogen could reach to an inapplicable size.

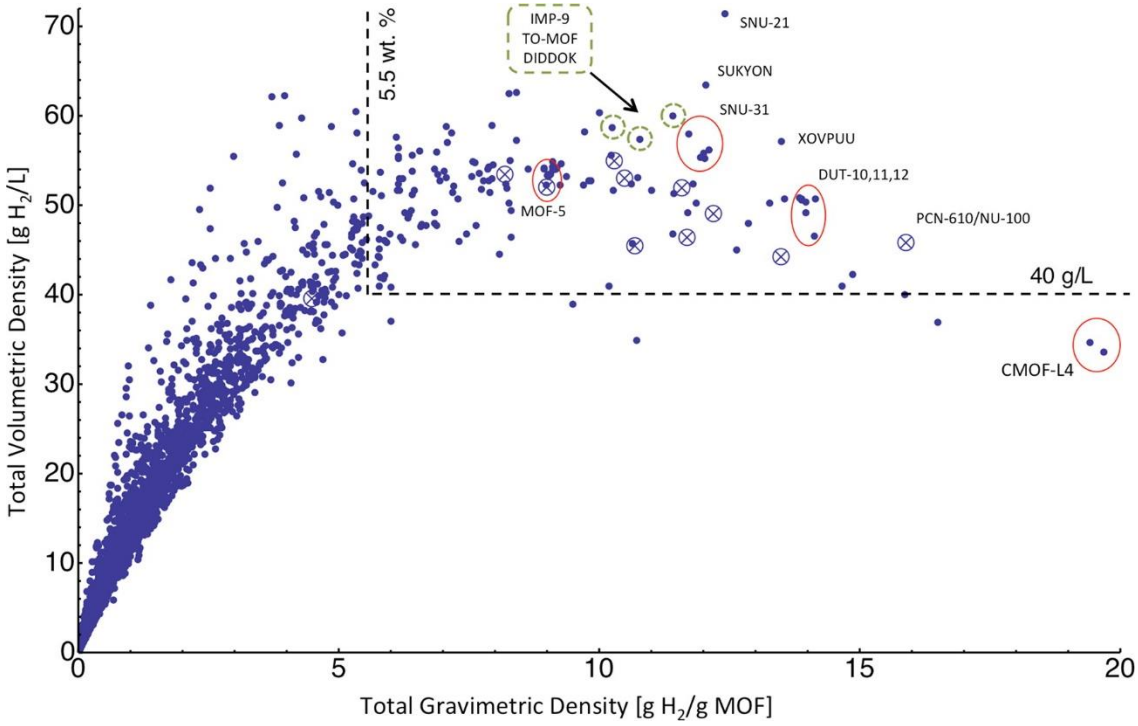

Figure 7. Theoretical total volumetric versus total gravimetric hydrogen adsorption capacities of several MOFs mined from Cambridge Structural Database (CSD). (Reprinted with permission from Ref. [17], copyright © 2013 American Chemical Society)

Hydrogen adsorption experiments for MOFs are usually done gravimetrically for practical reasons because mass of the samples can be determined easily. Although the volume could also be determined experimentally, the common practice is to convert the gravimetric uptake to volumetric uptake using the crystal density obtained by crystallographic experiments. This method allows researchers to have point by point comparison, however, the real volumetric capacity decreases as much as the decrease in packing density due to the void space between the crystals. Methods to increase packing density has been studied by different researchers. Applying physical force on MOF crystals helped increase the volumetric capacity up to a threshold in expense of decrease

in gravimetric density.[18,19] Another approach to tackle the void space problem was proposed to apply sol-gel synthesis to MOFs, which was reported to be successful on HKUST-1 (HKUST refers to The Hong Kong University of Science and Technology) and increased the volumetric uptake significantly compared to physical densification methods.[20]

1.2.1.1.4. Isosteric Heat of Adsorption

Enthalpy of interaction between the MOF surface and the hydrogen molecule describes how strongly hydrogen molecules bind to the surface in terms of energy. To achieve the best possible storage operation, heat of adsorption (Q_{st}) needs to be at an optimal value. For effective adsorption-desorption cycles at ambient temperatures and reasonable pressures, the value was estimated to be 15.1 and 20 kJ/mol by different researchers.[21,22] These values in the boundaries of hydrogen bonding, show the necessity of establishing strong interactions between the hydrogen and the MOF surface for optimal storage. Experimentally obtained Q_{st} of MOFs range from 4 to 12 kJ/mol, with the majority being at 6 – 7 kJ/mol range.[13]

Using the Clausius–Clapeyron relation, the heat of adsorption of hydrogen on the MOF surface could be obtained as a function of the amount of hydrogen adsorbed.[23]

$$-Q_{st} = RT^2 \left(\frac{\partial\, ln\, P}{\partial T}\right)_n \qquad (3)$$

Adsorption isotherms at two different temperatures are expressed as polynomials and interpolated. The slope of plot of *ln P* versus *1/T* gives $-Q_{st}/R$ as a function of *n*.

Largest value of Q_{st} is obtained at *n=0*, called zero-coverage enthalpy, where hydrogen binds to the strongest interaction site. After filling of the strongest binding site, then the enthalpy usually drops down until the pores are filled with hydrogen. Because only the zero-coverage enthalpy is reported, it does not always translate to higher adsorption since other structural parameters like pore size also play role in determining storage capacity. Nevertheless, increasing Q_{st} is an important challenge for MOFs to become viable hydrogen storage materials.

CHAPTER II

METAL ORGANIC FRAMEWORKS WITH SPECIAL TOPOLOGY AND OPEN METAL SITES FOR IMPROVED HYDROGEN ADSORPTION

Open metal sites in MOFs have been widely applied to enhance surface-guest interactions.[24,25] Open metals sites are found responsible for significant increase in low pressure hydrogen uptake as well as increase in zero-coverage enthalpy. Variety of transition metals including Co, Ni, Zn and Cu are incorporated in MOFs to have open metal sites, mostly studied metal being Cu due to ease of growing larger crystals stable enough to study the material. Creation of open metal sites is generally done via a process called activation, mainly composed of heating the material under vacuum at a certain temperature to remove the guest molecules, including the ones directly coordinated to the metal sites, leaving the metal with fewer coordination. Cu clusters with fewer coordination numbers are known to be stable due to help from Jahn-Teller distortion, as a result, MOFs with open Cu sites are very common. Removal of the guests to create Cu open metal sites can be observed easily by the color change of the crystals usually from light blue to violet.

Apart from existence of open metal sites, their orientation is also demonstrated very important to enhance the MOF-hydrogen interactions. Two MOFs, PCN-12 and PCN-12' are reported by our group show significant difference in low pressure hydrogen uptake, mainly attributed to alignment of the open metal sites.[14] Constructed by the same 5,5'-methylene diisophthalate ligand and the same di-copper paddlewheel metal cluster, they differ in packing due to different orientation of the ligand which resulted in having

open metal sites directly pointed towards the cages in the case of PCN-12, however, open metal sites in PCN-12' are not directly pointing towards the cages (Figure 8).

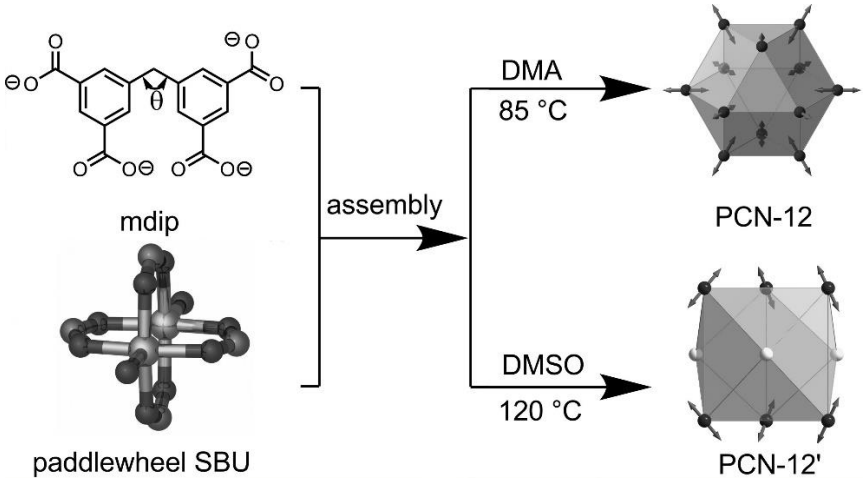

Figure 8. Synthesis conditions and open metal site alignment in PCN-12 and PCN-12' (Reproduced with permission from reference [[26]], Copyright 2008 John Wiley and Sons)

Due to its unique alignment of open Cu sites and optimal cage structure, PCN-12 was reported to be one of the highest hydrogen uptake MOFs at 77 K and under 1 atm.[13] Even though its promising hydrogen uptake at low pressure regime, its study is not fully developed albeit due to possible synthetic challenges during its solvothermal synthesis due to possibility of formation of PCN-12' or amorphous phases as the side products.

CHAPTER III

A FACILE SOLVOTHERMAL SYNTHESIS METHOD FOR PCN-12 WITH HIGH CRYSTALLINITY

3.1. Introduction

Obtaining highly crystalline samples with scalable synthesis methods could open new study directions to functional materials. Famous MOFs like HKUST-1, MOF-5, UiO-66 and PCN-250 are among the widely studied MOFs not only because they have unique properties, but also because of their easily scalable synthesis procedures and simpler ingredients which make them applicable to researchers from other fields potentially unfamiliar to MOF synthesis.[27,7] Therefore, development of easily applicable procedures to synthesize highly crystalline MOFs are of the uttermost importance. Although a promising MOF, originally reported conditions for solvothermal synthesis of PCN-12 which involves usage of sealed Pyrex tubes under vacuum and controlled slow heating/cooling could potentially hinder its further study.

A method to grow large single crystals of variety of Fe and Co μ_3-oxo cluster has been developed by our group utilizes introduction of mono carboxylate ligands called modulating reagents.[7] The method takes the kinetics of MOF crystal growth into account with the optimized amount of modulating reagent yields the largest size of crystals.

In this work, we have developed a facile method to grow highly crystalline PCN-12 samples with high yield to study this promising hydrogen storage material by addition of optimized amount of nitric acid to regulate the crystal growth process. The effect of incremental additions of nitric acid is also demonstrated. Powder diffraction studies and

adsorptive behavior of the samples are in agreement to show the effect of crystallinity on hydrogen storage capacity. In addition, hydrogen storage behavior of PCN-12 under high pressure regime and adsorption enthalpy experiments are also studied to investigate its potential as hydrogen storage material.

3.2. Experimental Section

3.2.1. Materials and Instrumentation

3.2.1.1. Materials

N,N-dimethyl acetamide (DMA), dimethyl sulfoxide (DMSO), methanol, dichloromethane, $Cu(NO_3)_2 \cdot 2.5\ H_2O$, isophthalic acid, paraformaldehyde, nitric acid (70%) and fuming sulfuric acid (20 – 24%), sodium hydroxide and hydrochloric acid were all purchased from commercially available sources and used without further purification.

3.2.1.2. Instrumentation

^{1}H-NMR data were collected on a Mercury 300 MHz NMR spectrometer. TGA data were obtained on a TGA-50 (SHIMADZU) thermogravimetric analyzer with a heating rate of 3 °C/min under nitrogen atmosphere. The powder X-ray diffraction patterns (PXRD) were recorded on a BRUKER D8-Focus Bragg-Brentano X-ray Powder Diffractometer equipped with a Cu sealed tube ($\lambda = 1.54178$ Å) at room temperature. Low-pressure gas adsorption measurements are done on a Micromeritics ASAP-2020 and ASAP-2420, and high-pressure hydrogen adsorption measurements are done on a Micromeritics Particulate Systems HPVA II. Ultra-high purity grade (99.999%) N_2 and H_2 were used for all measurements.

3.2.2. Synthesis of 3,3',5,5'-tetracarbomethoxydiphenylmethane (H_4mdip)

The synthesis is derived from the literature.[28] 33 grams (0.20 mol) of isophthalic acid and 3.1 grams of paraformaldehyde (0.10 mol) were dissolved in 100 ml of fuming sulfuric acid (20-24%). The resulting solution was refluxed at 115 °C overnight. After cooled down, it was carefully poured on chilled water and forming precipitate was filtered. Then, the solid was hydrolyzed either with hydrochloric acid in methanol or with sodium hydroxide in methanol and acidified with hydrochloric acid in methanol. Then the product is filtered and dried, and then recrystallized from ethyl acetate (yield: 16.0 grams, 0.047 mol, 47%). ^{1}H NMR (300 MHz, DMSO-D6) δ 4.28 (s, 2H), δ 8.08 (s, 4H), δ 8.31 (s, 2H), δ 13.26 (s, 4H).

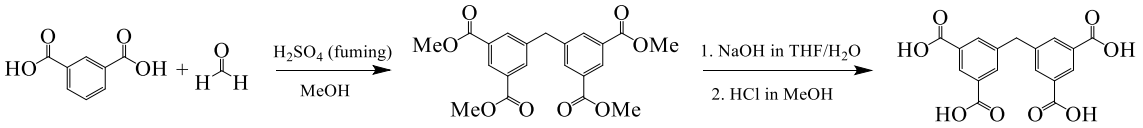

Scheme 1. Synthesis of **H_4mdip**.

3.2.3. Synthesis of PCN-12

PCN-12 crystals were synthesized in a 4 mL vial laid on its side; 8 mg H_4mdip, 21 mg $Cu(NO_3)_2 \cdot 2.5\ H_2O$ and in the range of 0 and 0.15 mL HNO_3 is dissolved in 4 mL DMA and placed in an oven at 85 °C. After 5 – 7 days, blue square prism crystals were washed with DMA and then collected by decanting (yield: 9 mg after activation, 79% based on H_4mdip).

Table 2. Synthesis conditions of PCN-12 with increasing HNO_3 ratios

	$CuNO_3 \cdot 2.5\ H_2O$			H_4mdip			HNO_3			DMA
ID	eq	mmol	mg	eq	mmol	mg	eq	mmol	mL	mL
1	3.9	0.09	21	1	0.02	8	0	0.0	0	4
2	3.9	0.09	21	1	0.02	8	34	0.8	0.05	4
3	3.9	0.09	21	1	0.02	8	68	1.6	0.1	4
4	3.9	0.09	21	1	0.02	8	102	2.4	0.15	4
5	3.9	0.09	21	1	0.02	8	136	3.2	0.2	4

3.2.4. Synthesis of PCN-12'

Like PCN-12 synthesis, PCN-12' crystals were also synthesized in vials laying down. 8 mg H_4mdip, 21 mg $Cu(NO_3)_2 \cdot 2.5\ H_2O$ and in the range of 0 and 0.04 mL HNO_3 is dissolved in 4 mL DMSO and placed in an oven at 120 °C. After 3 days, blue square prism crystals were washed with DMSO and then collected by decanting (yield: 3.6 mg after activation, 53% based on H_4mdip).

Table 3. Synthesis conditions of PCN-12' with increasing HNO_3 ratios

	$CuNO_3 \cdot 2.5\ H_2O$			H_4mdip			HNO_3			DMSO
ID	eq	mmol	mg	eq	mmol	mg	eq	mmol	mL	mL
1	3.9	0.09	21	1	0.02	8	0	0.0	0	4
2	3.9	0.09	21	1	0.02	8	7	0.2	0.01	4
3	3.9	0.09	21	1	0.02	8	14	0.3	0.02	4
4	3.9	0.09	21	1	0.02	8	20	0.5	0.03	4
5	3.9	0.09	21	1	0.02	8	27	0.6	0.04	4

3.2.5. Low-pressure gas adsorption measurements

Synthesized samples of PCN-12 and PCN-12' are washed several times with DMA, and then solvent exchanged first with methanol and then with DCM before activation. While soaked in DCM, samples were transferred to the test tubes of porosity analyzer and DCM was removed by vacuuming using the Schlenk line and then charged with nitrogen before transferring to porosity analyzer to prevent exposing the dry sample to air. After removal of DCM, the samples were activated using the degas function of porosity analyzer for 6 hours at different temperatures in the range of 100 °C and 180 °C. Alternatively, supercritical CO_2 was also used to compare against activation by degassing.

3.3. Results and Discussion

3.3.1. PCN-12 and PCN-12' Synthesis

Placing vials horizontal is a crucial detail to obtain highly crystalline samples, as the crystals are found to grow on the vial surface first, and once the surface is covered then additional powder is formed. Horizontal placement increases available vial surface to increase yield of highly crystalline product. Scaling up the solvothermal synthesis by using larger volume vials or placing the vials vertically is found to decrease crystallinity and resulted in lower quality samples, therefore, all experiments are done applying the same method. Adding more nitric acid (more than 0.2 mL (136 eq.) for PCN-12 and 0.04 mL (27 eq.) for PCN-12') was found to prevent crystal formation within two weeks (Figure 9).

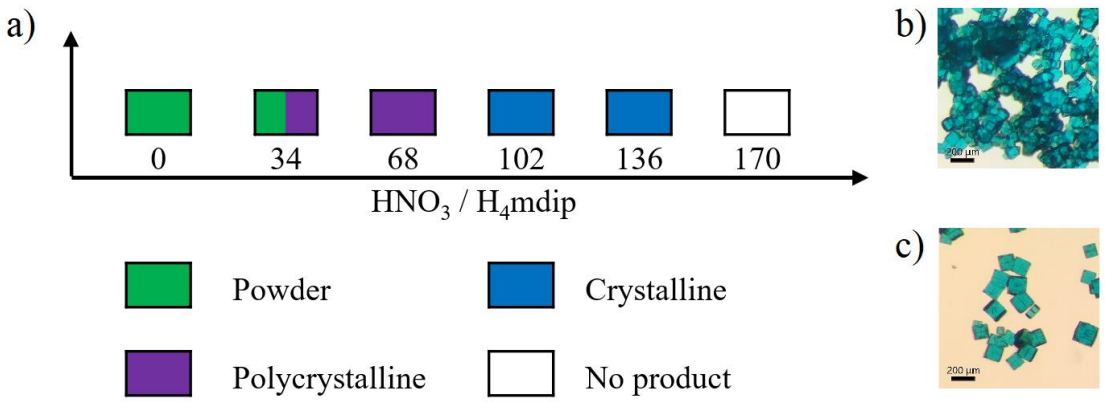

Figure 9. Crystallization diagram of PCN-12 with increasing NHO_3 ratios (a) and optical images of polycrystalline and highly crystalline samples with HNO_3/H_4mdip ratios of 68 (b) and 102 (c).

Entries with above 170 eq. HNO_3 were omitted for clarity, as none of them yielded any solid product. A very similar phenomenon is observed with crystal growth process of PCN-12' with smaller HNO_3/H_4mdip ratios where the sample with 35 eq. HNO_3 did not yield any product and the sample with 27 eq. HNO_3 yielded the best crystals. PCN-12' samples synthesized with the highest crystallinity is tested to compare them to the best performing PCN-12 samples, however, intermediate samples were not tested further.

3.3.2. PXRD Studies

Powder X-Ray diffraction patterns indicate formation of the same crystalline structure with comparable signal intensities (Figure 10). Approximately the same amount of sample (10 mg) and the same settings were used for diffraction, so relatively poor diffraction of 0 eq. HNO_3 sample shows that the sample has a relatively greater degree of amorphousness.

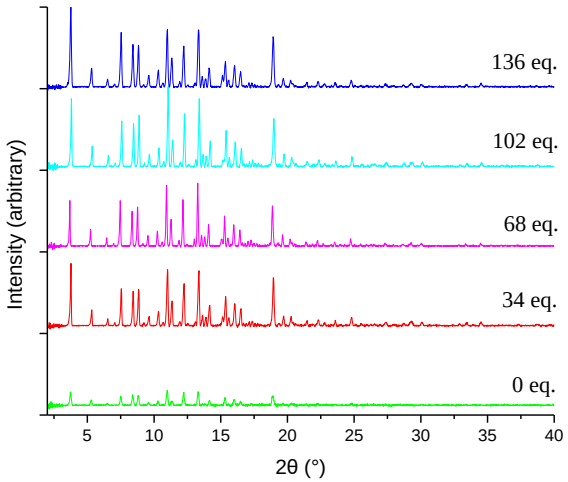

Figure 10. PXRD patterns of PCN-12 samples synthesized using different ratios of HNO_3/H_4mdip.

In order to confirm the structures are indeed PCN-12 and PCN-12', PXRD patterns are plotted against simulated patterns using the reported structures found on CCDC database (Figure 11). Although majority of the signals match, there are discrepancies associated with crystals not being oriented randomly, causing some of the signal intensities not matching well with the simulated patterns. Grinding the crystals resulted in loss of signals and was avoided to be able to use the same samples in gas sorption studies. For PCN-12' sample, signals close to 8 and 10° are extremely weak.

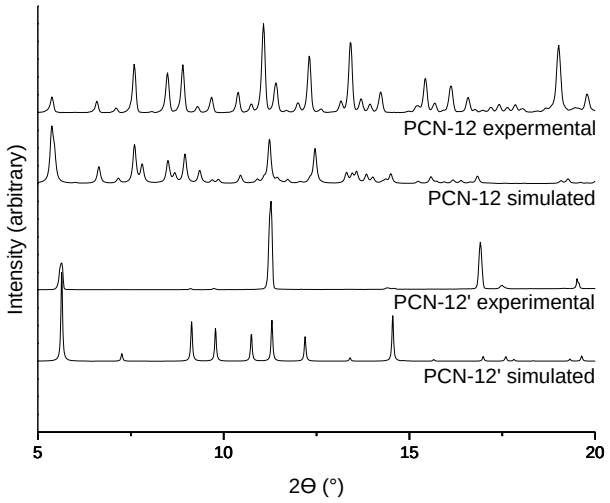

Figure 11. PXRD patterns of synthesized PCN-12 and PCN-12' (136 eq. and 27 eq. samples respectively) and simulated patterns of PCN-12 and PCN-12'.

3.3.3. Gas Sorption Studies

Nitrogen adsorption studies were conducted to evaluate the porosity of PCN-12 samples. Adsorbed nitrogen amount was found to increase with increasing HNO_3 equivalences, matching well with PXRD and optical image results (Figure 12). Samples made with in the range of 0 and 68 equivalences of NHO_3 show linearly increasing nitrogen uptake, while 102 and 136 eq. samples are almost identical. All isotherms are type I without any hysteresis towards $P/P_0 = 1$, indicating that all samples are microporous with no mesoporous or macroporous content. Based on the PXRD results combined with the nitrogen isotherms, the composition of the samples is speculated as a combination of porous PCN-12 and non-porous amorphous solid which decrease overall specific surface area.

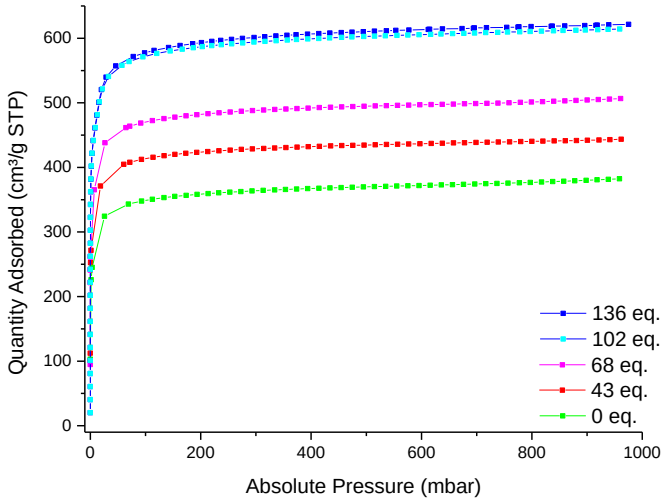

Figure 12. Nitrogen adsorption isotherms of PCN-12 samples synthesized using different ratios of HNO_3/H_4mdip at 77 K.

The BET surface areas of the samples are calculated, and the same increasing order was found as expected. While powder and polycrystalline samples have increasing surface area, crystalline samples have almost identical results. Even though the samples with 43 and 68 eq. HNO_3 show high crystallinity with strong signals based on PXRD results, their porosity and surface areas are significantly lower than crystalline samples with 102 and 163 HNO_3 equivalences.

Low-pressure hydrogen adsorption isotherms are correlated to nitrogen adsorption isotherms and calculated BET surface areas of the samples, powder and polycrystalline samples have linearly increased hydrogen adsorption and both crystalline samples have the highest and similar values (Figure 13).

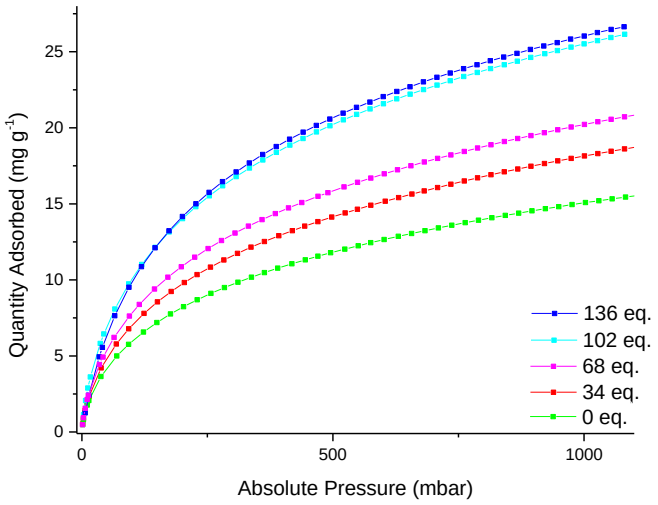

Figure 13. Hydrogen adsorption isotherms of PCN-12 samples synthesized using different ratios of HNO_3/H_4mdip at 77 K.

BET surface areas and the hydrogen uptakes at 1 bar are summarized in the Table 4 show that among synthesized PCN-12 samples there is a strong correlation between the surface area of the sample and its hydrogen uptake, the correlation is shown in Figure 14.

Table 4. BET surface areas and H_2 uptake of PCN-12 samples at 77 K and 1 bar.

HNO_3/H_4mdip	BET Surface Area (m^2 g^{-1})	H_2 Uptake at 1 bar and 77 K (mg g^{-1})
136	2285 ± 8	26.3
102	2216 ± 14	25.7
68	1889 ± 14	20.4
43	1663 ± 8	18.3
0	1408 ± 7	15.2

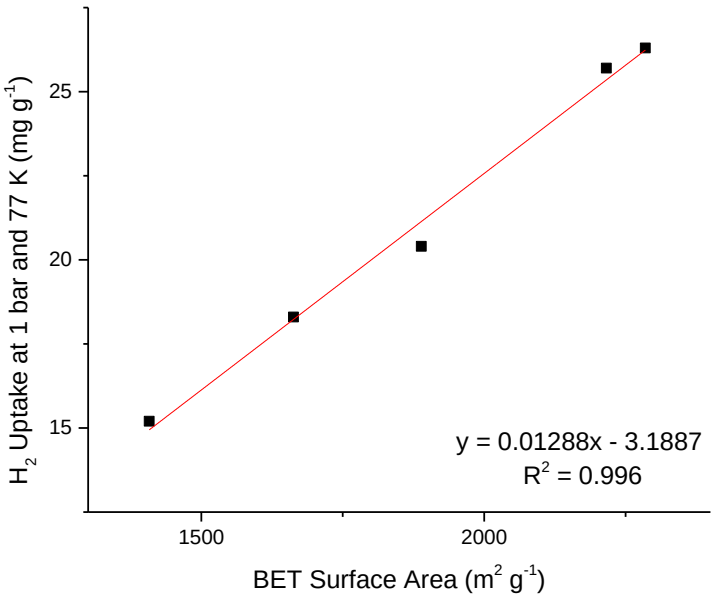

Figure 14. BET surface area versus hydrogen uptake at 1 bar and 77 K of PCN-12 samples synthesized. The relationship is found as linear.

Optimizing the activation condition is an important procedure detail to obtain the highest possible hydrogen uptake of the sample, as removal of the solvent molecules within the pores are done by activation process. The optimal temperature is found where all the solvent and the coordinated water molecules on the open metal sites are removed while the structural integrity of the material is preserved. Activation conditions that yield the best hydrogen uptake is also investigated and temperatures ranging from 120 °C to 180 °C are found to be the optimal range based on low-pressure hydrogen adsorption tests. Activation at 100 °C is speculated to be insufficient to remove the axial water molecules on open Cu sites. Activation by using supercritical CO_2 to remove solvent molecules did result in decrease in hydrogen uptake, most probably because of short exposure of samples

to air during handling after activation (Figure 15). Slow decomposition of relatively labile MOFs are commonly known and its implications on hydrogen adsorption is previously studied on MOF-5.[9] Long exposure of PCN-12 to air after activation causes permanent color change from violet to turquoise/green that is not recoverable by reactivating and the porosity is found to decrease gradually.

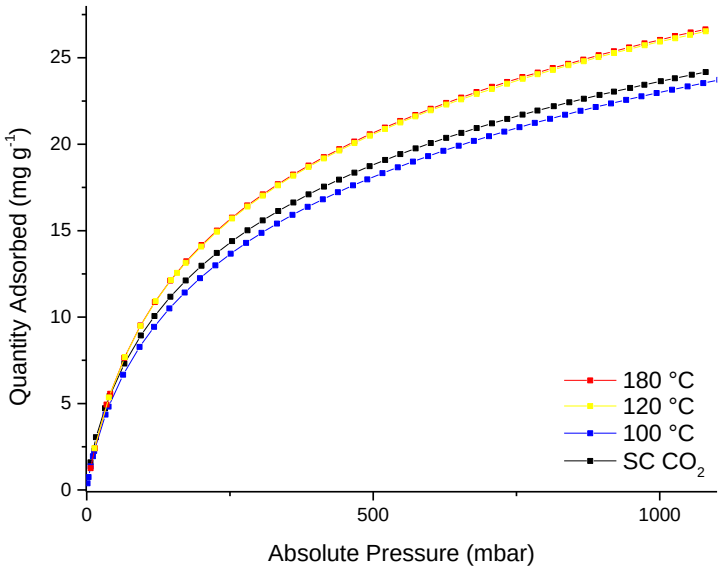

Figure 15. Low pressure hydrogen uptake of PCN-12 samples (136 HNO_3/H_4mdip) activated at different conditions. Sample activated at 180 °C (red) is almost identical to 120 °C sample (yellow). Measurements between 120 ° and 180 °C are omitted for clarity.

While low-pressure hydrogen adsorption isotherms show the strength of MOF-hydrogen interaction, the pores of the MOFs are not usually saturated with hydrogen under 1 bar and 77 K. For on-board storage usage, pressures up to 100 bars are considered applicable, which is also usually enough to saturate the MOF surface with hydrogen usually indicated by the excess uptake reaching a maximum. High-pressure hydrogen

adsorption of crystalline and polycrystalline PCN-12 samples (Figure 16) show an expected difference correlated to the surface area difference of the samples. Both samples reach their maximum excess uptake at around 40 bars, which would be expected by materials with a similar pore structure.

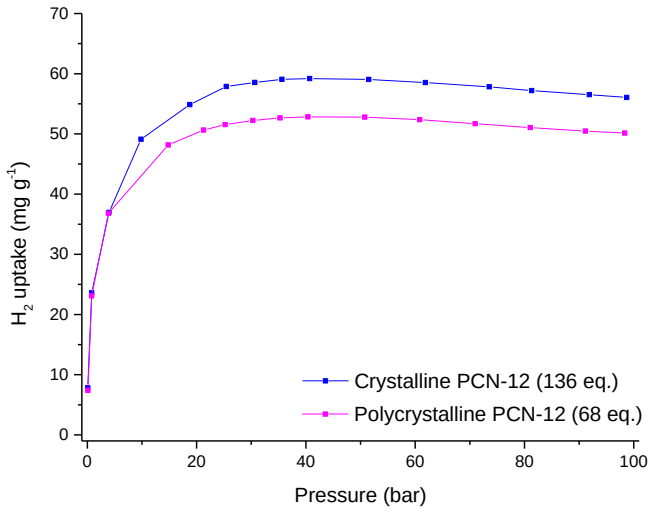

Figure 16. Gravimetric excess high-pressure hydrogen adsorption isotherms of polycrystalline and crystalline PCN-12 samples at 77 K. Highest uptakes of crystalline and polycrystalline samples are 59.2 mg g^{-1} (at 40.7 bar) and 52.8 mg g^{-1} (at 40.3 bar) respectively.

Using the adsorption isotherms at two different temperatures (77 K and 87 K, Figure 17), adsorption enthalpy of crystalline and polycrystalline PCN-12 samples were calculated by applying Clausius–Clapeyron relation as a function of surface coverage (Figure 18). Temperatures at 77 K and 87 K are maintained by placing samples in dewars filled with liquid nitrogen or liquid argon.

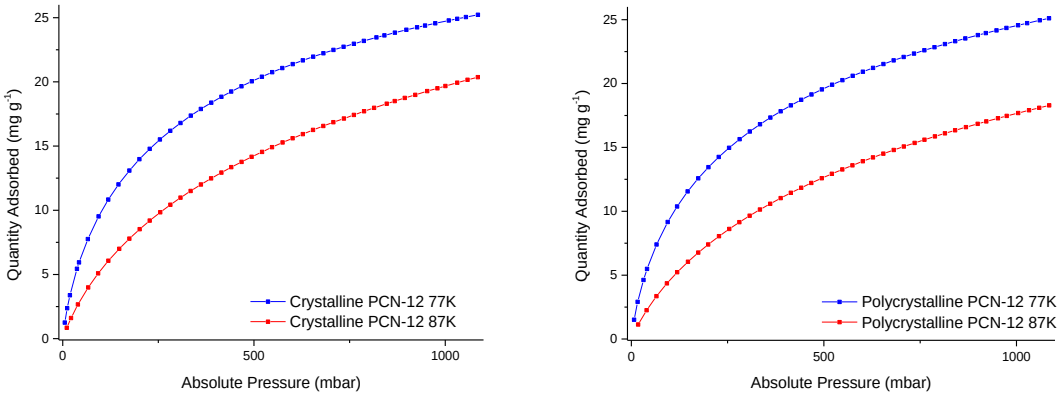

Figure 17. Hydrogen adsorption isotherms of crystalline (left) and polycrystalline (right) PCN-12 samples (136 and 68 HNO_3 eq. samples, respectively) at 77 and 87 K.

Adsorption enthalpy of hydrogen on crystalline and polycrystalline PCN-12 samples were calculated to be 7.2 and 6.3 kJ mol^{-1} at zero-coverage, showing 0.9 kJ mol^{-1} difference. The values gradually drop to 5.4 and 4.5 kJ mol^{-1} at 2.0 H_2/Cu surface coverage. With the assumption that available adsorption surface is solely composed of PCN-12 pores, the difference of Q_{st} values at zero-coverage suggests that at 77 - 87 K range open Cu sites are not exclusive adsorption sites. It is worth noting that the two minor steps down at 0.35 and 0.70 H_2/Cu coverage could be associated to two different types of MOF-hydrogen interactions present, however, this data alone is not sufficient for further conclusions.

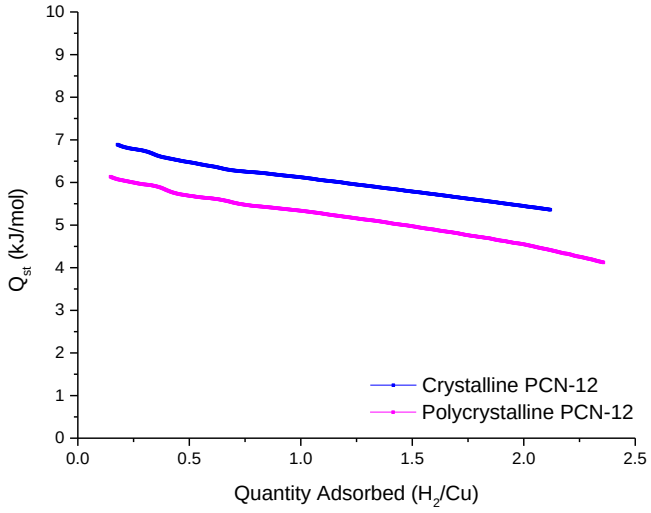

Figure 18. Hydrogen heat of adsorption (Q_{st}) versus open metal site coverage of crystalline and polycrystalline PCN-12 samples calculated using 77 K and 87 K hydrogen adsorption isotherms. At zero coverage, crystalline and polycrystalline PCN-12 samples have Q_{st} of 7.2 and 6.3 kJ/mol estimated respectively.

Finally, high-pressure hydrogen adsorptions of the best performing PCN-12 and PCN-12' samples (Figure 19 and 20) are tested and compared to evaluate their performances for possible on-board applications. The excess uptake data is obtained gravimetrically and converted to volumetric uptake using crystal density with the assumption that the all available volume in a container is filled with a perfectly packed crystal, so the real excess volumetric uptake is going to be lowered with the efficiency of packing density of the crystals. The total uptakes are calculated using the experimentally obtained pore volume and the density of the hydrogen at the corresponding pressure and temperature. This calculation ignores the possible pore volume reduction because of the additional volume spanned by the adsorbed hydrogen within the pores already accounted for by excess uptake, however, this amount cannot be estimated accurately since the

adsorbed hydrogen in the pores will behave differently and may span a different volume than the hydrogen in the gas phase. The difference in gravimetric total uptakes of PCN-12 and PCN-12' is lessened with the difference in volumetric total uptakes due to higher crystal density of PCN-12', which is an expected tradeoff between higher and lower density MOFs.

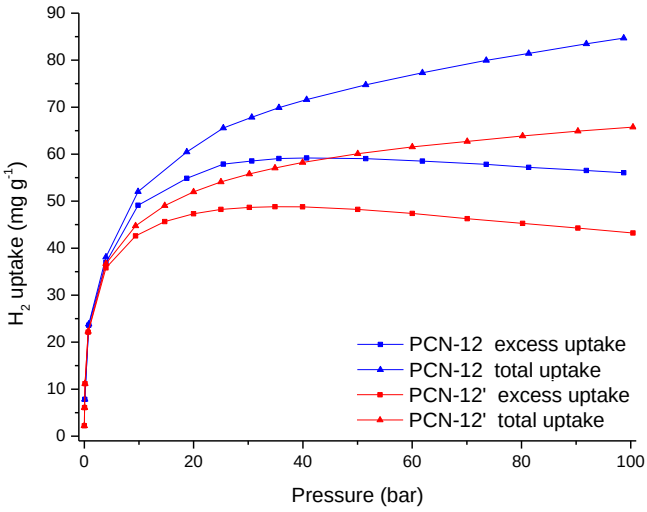

Figure 19. Gravimetric high-pressure hydrogen adsorption isotherms of PCN-12 and PCN-12' at 77 K. Highest excess uptakes for PCN-12 and PCN-12' are 59.2 mg g^{-1} (at 40.7 bar) and 48.8 mg g^{-1} (at 34.9 bar), total uptakes reach up to 84.7 mg g^{-1} and 65.8 mg g^{-1} at 100 bars, respectively.

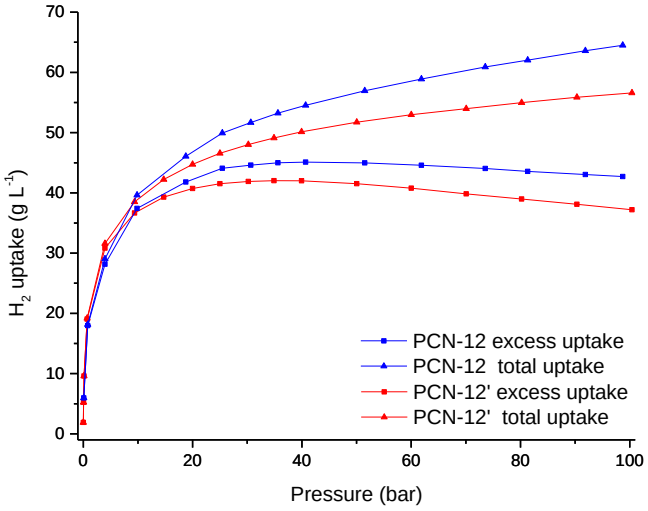

Figure 20. Volumetric high-pressure hydrogen adsorption isotherms of PCN-12 and PCN-12' at 77 K. Highest excess uptakes for PCN-12 and PCN-12' are 45.1 g L^{-1} (at 40.7 bar) and 42.0 g L^{-1} (at 34.9 bar), total uptakes reach up to 64.5 g L^{-1} and 56.6 g L^{-1} at 100 bars, respectively.

3.4. Conclusions

Overall, a facile synthesis method for PCN-12 that yield high quality and large crystals by addition of HNO_3 to solution of metal and ligand was demonstrated and optimized. The method is found applicable to synthesis of PCN-12' as well. The effect of adding different amounts of HNO_3 on crystal formation of PCN-12 and its implications on porosity and hydrogen storage performance were studied. This method removes the necessity of using Pyrex vials sealed under inert atmosphere and tedious heating-cooling process during solvothermal synthesis and helps studying PCN-12 structure easier for future studies. Finally, hydrogen storage performance of PCN-12 and PCN-12' using this synthesis methods were compared. PCN-12 was shown to be a promising hydrogen storage material with 59.2 mg g^{-1} gravimetric and 45.1 g L^{-1} volumetric excess hydrogen uptakes as well as 84.7 mg g^{-1} gravimetric and 64.5 g L^{-1} volumetric total hydrogen uptakes at 77 K.

CHAPTER IV

TOWARD SYNTHESIS OF PCN-12 BASED MOFS

4.1. Introduction

Besides well oriented open metal sites and optimal topology, tuning the ligand environment has been proven successful to increase hydrogen storage capacity of MOFs. Recently Schröder et. al. has shown that constructing the MOF with ligands containing anthracene rings increases the hydrogen uptake significantly, due to strong interaction between the anthracene ring and hydrogen within the pores.[29] The neutron diffraction studies found that anthracene is responsible for its relatively higher hydrogen uptake when compared to non-anthracene version of the same structure. Alternatively, it was demonstrated that incorporating triazole rings in the ligand helped polarizing the pores along with open metal sites and increased the hydrogen uptake via a different phenomenon.[30] In a study more related to PCN-12, different MOFs isoreticular to PCN-12 containing group 14 elements in replacement of the central carbon of the ligand (Si and Ge) were tested and found that low-pressure hydrogen adsorption as well as adsorption enthalpy increase (Ge > Si > C).[31] Moreover, an isoreticular MOF to PCN-12 was reported with ketone functionalized ligand (H_4cdip) by replacing the central CH_2 with a carbonyl (C=O) and has shown 2.8 wt.% hydrogen uptake under 1 bar and 77 K.[32]

In light of these studies, hydrogen adsorption could be increased further by tuning the ligand environment. For this purpose, a PCN-12 based MOF with alternative ligand (Figure 21) was proposed by changing the coordinating carboxylates with tetrazolates.

Usage of multiple highly electronegative atoms like nitrogen in the ligand could help polarize the pore environment and increase the strength of MOF-hydrogen interactions.

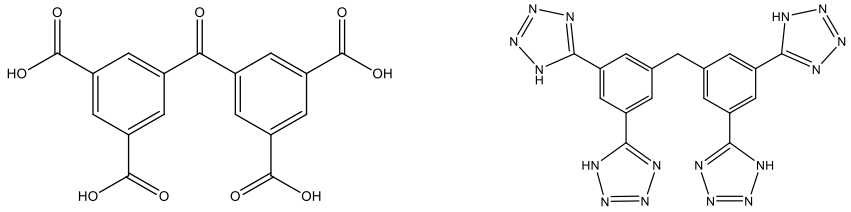

Figure 21. Alternative ligands to 5,5'-methylene diisophthalate (H_4mdip) to tune the pore environment. 5,5'-carbonyl diisophthalic acid (H_4cdip, left) and bis(3,5-di(1H-tetrazol-5-yl)phenyl)methane (H_4bdtpm, right).

4.2. Experimental Section

4.2.1. Materials and Instrumentation

4.2.1.1. Materials

All chemicals used as starting materials including N,N-dimethyl acetamide (DMA), dimethyl sulfoxide (DMSO), methanol, dichloromethane, $CuSO_4 \cdot 5\,H_2O$, NaCN, 1,3,5-tribromobenzene, diethyl ether, n-butyllithium and hydrochloric acid were all purchased from commercially available sources and used without further purification. *Caution! Although no incidents have occurred while handling of n-butyllithium during these studies, the compound is known to be extremely flammable, igniting imminently upon exposure to air. It must be handled under inert atmosphere using only previously inspected syringe or cannula. NaCN is known to be extremely toxic upon ingestion, may from an extremely toxic gas (HCN) when introduced to acidic media. It must be handled under*

well ventilated fume hood with great care, and after used, the excess amount must be detoxified using a chemical such as KSCN.

4.2.1.2. Instrumentation

^{1}H-NMR data were collected on a Mercury 300 MHz NMR spectrometer. Mass spectrometry data were collected on commercially available matrix-assisted laser desorption/ionization (MALDI) time-of-flight (TOF) mass spectrometer. ACD-NMR Processor Academic Edition was used to analyze ^{1}H-NMR data.

4.2.2. Synthesis of bis(3,5-di(1H-tetrazol-5-yl)phenyl)methane (H_4bdtpm)

The synthesis was achieved applying the synthetic procedures respectively.[33,34,35] Except the final structure (H_4bdtpm), the structures are reported with common characterization methods which match well with the results reported in this work.

4.2.2.1. Synthesis of bis(3,5-dibromophenyl)methanol (Step 1)

28.3 grams (90 mmol) 1,3,5-tribromobenzene was dissolved in 600 mL diethyl ether previously dried in a solvent purification system and then cooled down to -178 °C and degassed for 2 hours. Then 36 mL (90 mmol) n-butyllithium was added to the flask through a syringe and allowed to mix over an hour. Then 2.7 mL (44 mmol) methyl formate was added through a syringe and then the mixture was allowed to reach room temperature and stirred under nitrogen atmosphere for 16 hours. The reaction was quenched by adding first 600 mL of water and then 10 mL of 36% HCl dissolved in 200 mL of water. The product was extracted with diethyl ether (200 mL x 3 times). The product

is obtained after removal of diethyl ether by rotovap, washed with hexanes and then dried in oven overnight (yield: 7.5 g, 15 mmol, 33%). ^{1}H NMR (300 MHz, $CDCl_3$) δ 2.35 (s, 1H), δ 5.69 (s, 1H), δ 7.44 (s, 4H), δ 7.61 (s, 2H).

4.2.2.2. Synthesis of bis(3,5-dibromophenyl)methane (Step 2)

7.5 grams (15 mmol) of bis(3,5-dibromophenyl)methanol, 1.5 grams (48 mmol) of red phosphorous and 0.75 gram (3.0 mmol) of iodine were dissolved in 180 mL of glacial acetic acid. Then the mixture was heated to 115 °C under nitrogen atmosphere and refluxed for 72 hours. The mixture was allowed to cool down and addition of water yielded a mixture of light-yellow product and the remaining red phosphorous. The product is recovered from 600 mL DCM it was dissolved to separate from the red phosphorous (yield: 3.0 g, 0.62 mmol, 41%). ^{1}H NMR (300 MHz, $CDCl_3$) δ 3.85 (s, 2H), δ 7.24 (s, 4H), δ 7.56 (s, 2H).

4.2.2.3. Synthesis of 5,5'-methylenediisophthalonitrile (Step 3)

2.90 grams (6mmol, 1 eq.) of bis(3,5-dibromophenyl)methane, 2.11 grams (24 mmol, 4 eq.) of 1,2-dimethylethylenediamine, 0.46 gram (2.4 mmol, 0.4 eq.) of CuI, 0.80 gram (4.8 mmol, 0.8 eq.) of KI and 1.47 grams (30 mmol, 5 eq.) of NaCN were mixed in 120 mL of toluene under nitrogen atmosphere. The mixture was heated to 130 °C and refluxed for 10 days. The reaction progress was monitored with ^{1}H NMR. Then the mixture was cooled down and a flush column was used to remove the remaining Cu complex in the solution. Then the dried yellow solid was recrystallized from DCM (yield:

0.63 gram, 0.24 mmol, 39%). ^{1}H NMR (300 MHz, $CDCl_3$) δ 4.18 (s, 2H), δ 7.69 (s, 4H), δ 7.91 (s, 2H).

4.2.2.4. Synthesis of bis(3,5-di(1H-tetrazol-5-yl)phenyl)methane (Step 4)

0.60 gram (2.2 mmol, 1 eq.) of 5,5'-methylenediisophthalonitrile and 7 milligrams ($2 \cdot 10^{-3}$ mmol, 2% eq.) of $CuSO_4 \cdot 5\ H_2O$ are dissolved in 2 mL of DMSO. Then 0.86 gram of NaN_3 was added to the mixture and color change was observed. The mixture was stirred for 48 hours and then 80 mL of 0.5 M HCl was added to precipitate the product. After cooling in an ice bath, the white solid was filtered out (yield: 0.90 gram, 2.2 mmol, 98%). ^{1}H NMR (300 MHz, DMSO-D6) δ 4.39 (s, 2H), δ 8.621 (s, 4H), δ 8.65 (s, 2H), δ 9.12 (s, 2H).

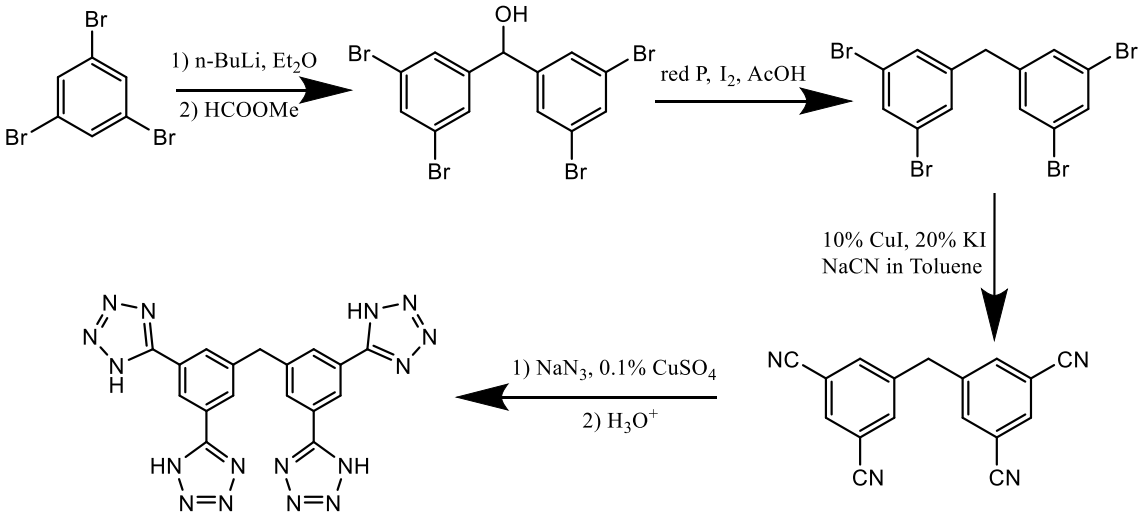

bis(3,5-di(1*H*-tetrazol-5-yl)phenyl)methane

Scheme 2. Synthesis of H_4bdtpm in 4 steps.

4.2.3. MOF Synthesis Attempts

Detailed screening studies to grow possible Cu MOFs using H_4bdtpm and Cu salts have failed to yield crystalline products. The conditions tried in DMA, DMF or DMSO are reported on a table in the following section. Conditions are derived from original synthesis conditions reported for PCN-12 and a Cu tetrazolate MOF reported.[36]

4.3. Results and Discussion

4.3.1. Ligand Synthesis and Characterization

The ligand (H_4bdtpm) was not found in the literature, searches on SciFinder® or Reaxys® returned with the message that the structure was not found the databases. The ^{1}H NMR and the mass spectrometry results were sufficient to identify the product.

The signal integration of the proton on the tetrazole ring was found lower than expected (Figure 22), however, presence of this proton is dependent on the acidity of the media. The signal intensity of the other protons matches well with the structure of H_4bdtpm.

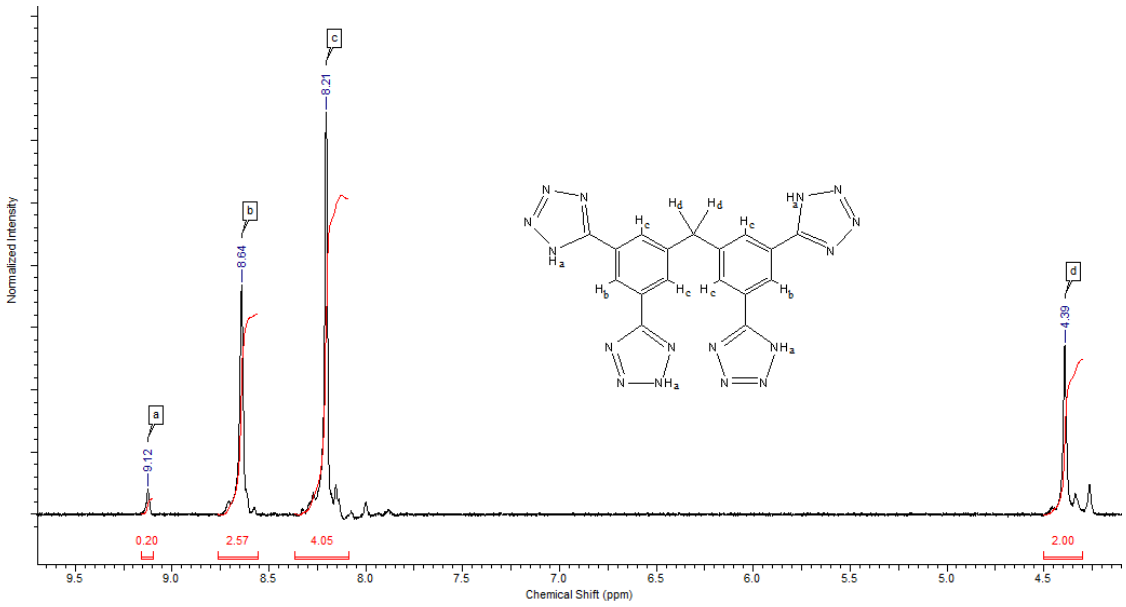

Figure 22. 1H NMR spectrum of H_4bdtpm in DMSO-D6. Each signal is assigned to a proton of the ligand.

The matrix-assisted laser desorption/ionization (MALDI) time-of-flight (TOF) mass spectrum of H_4bdtpm (Figure 23) has increased the confidence in success of the synthesis. Presence of Na(H_3bdtpm) is not surprising as with the incorporation of multiple tetrazole rings in the structure, H_4bdtpm is expected to have relatively stronger acidity, and under neutral conditions the monosodium salt could be present in a significant ratio.

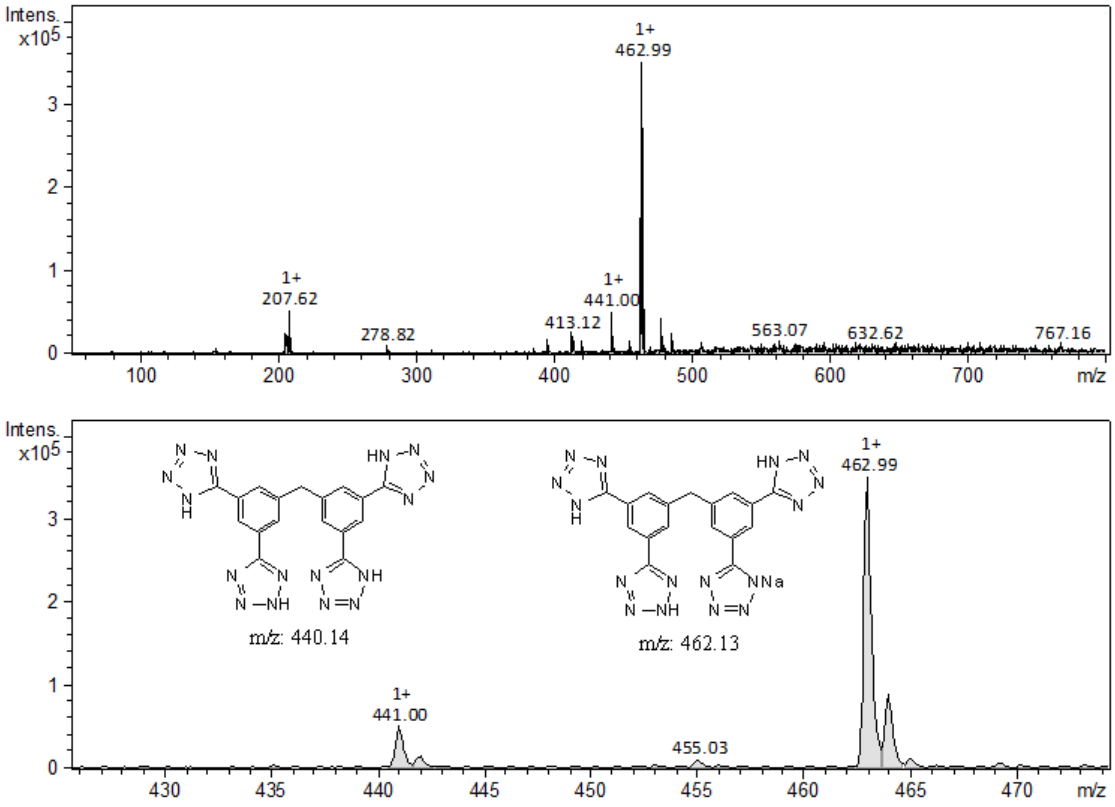

Figure 23. MALDI-TOF MS spectrum of H_4bdtpm. The major signals correspond to m/z of the ligand and the monosodium salt of the ligand.

4.3.2. MOF Growth Studies

The detailed conditions applied for solvothermal synthesis and their results are summarized in the table below.

Table 5. Details of solvothermal synthesis screening conditions and the result.

	$CuNO_3 \cdot 2.5\ H_2O$			H_4bdtpm			HNO_3			DMA	T	Result	
ID	eq	mmol	mg	eq	mmol	mg	eq	mmol	mL	mL	°C	Crystallinity	Color
1	7.6	0.17	40	1	0.023	10	0	0	0	4	85	Amorphous Powder	Blue-Green
2	7.6	0.17	40	1	0.023	10	34	0.8	0.1	4	85	Amorphous Powder	Blue-Green
3	7.6	0.17	40	1	0.023	10	68	1.6	0.2	4	85	Amorphous Powder	Blue-Green
4	7.6	0.17	40	1	0.023	10	102	2.4	0.3	4	85	Amorphous Powder	Blue-Green
5	7.6	0.17	40	1	0.023	10	136	3.2	0.4	4	85	Amorphous Powder	Blue-Green
6	7.6	0.17	40	1	0.023	10	170	4	0.5	4	85	Amorphous Powder	White
7	7.6	0.17	40	1	0.023	10	204	4.8	0.6	4	85	Amorphous Powder	White
8	7.6	0.17	40	1	0.023	10	238	5.6	0.7	4	85	Amorphous Powder	White
9	7.6	0.17	40	1	0.023	10	272	6.4	0.8	4	85	Amorphous Powder	White

	$CuNO_3 \cdot 2.5\ H_2O$			H_4bdtpm			HNO_3			DMF	T	Result	
ID	eq	mmol	mg	eq	mmol	mg	eq	mmol	mL	mL	°C	Crystallinity	Color
10	7.6	0.17	40	1	0.023	10	0	0	0	4	85	Amorphous Powder	Blue-Green
11	7.6	0.17	40	1	0.023	10	34	0.8	0.1	4	85	Amorphous Powder	Blue-Green
12	7.6	0.17	40	1	0.023	10	68	1.6	0.2	4	85	Amorphous Powder	Blue-Green
13	7.6	0.17	40	1	0.023	10	102	2.4	0.3	4	85	Amorphous Powder	Blue-Green
14	7.6	0.17	40	1	0.023	10	136	3.2	0.4	4	85	Amorphous Powder	Blue-Green
15	7.6	0.17	40	1	0.023	10	170	4	0.5	4	85	Amorphous Powder	White
16	7.6	0.17	40	1	0.023	10	204	4.8	0.6	4	85	Amorphous Powder	White
17	7.6	0.17	40	1	0.023	10	238	5.6	0.7	4	85	Amorphous Powder	White
18	7.6	0.17	40	1	0.023	10	272	6.4	0.8	4	85	Amorphous Powder	White

	$CuNO_3 \cdot 2.5\ H_2O$			H_4bdtpm			HNO_3			DMSO	T	Result	
ID	eq	mmol	mg	eq	mmol	mg	eq	mmol	mL	mL	°C	Crystallinity	Color
19	7.6	0.17	40	1	0.023	10	0	0	0	4	85	Amorphous Powder	Blue-Green
20	7.6	0.17	40	1	0.023	10	34	0.8	0.1	4	85	Amorphous Powder	Blue-Green
21	7.6	0.17	40	1	0.023	10	68	1.6	0.2	4	85	Amorphous Powder	Blue-Green
22	7.6	0.17	40	1	0.023	10	102	2.4	0.3	4	85	Amorphous Powder	Blue-Green
23	7.6	0.17	40	1	0.023	10	136	3.2	0.4	4	85	Amorphous Powder	Blue-Green
24	7.6	0.17	40	1	0.023	10	170	4	0.5	4	85	Amorphous Powder	Blue-Green
25	7.6	0.17	40	1	0.023	10	204	4.8	0.6	4	85	Amorphous Powder	White
26	7.6	0.17	40	1	0.023	10	238	5.6	0.7	4	85	Amorphous Powder	White
27	7.6	0.17	40	1	0.023	10	272	6.4	0.8	4	85	Amorphous Powder	White

4.4. Conclusions

The proposed ligand was synthesized successfully, however, a crystalline structure was unsuccessful despite using various conditions and methodology applicable to crystal growth of PCN-12. Expanding the screening parameters like temperature, different concentrations of the metal salt and the ligand could be helpful for successful crystal growth to be able to study possible structures by X-Ray diffraction and gas-sorption studies.

CHAPTER V

SUMMARY

In this thesis, a facile method for solvothermal synthesis of PCN-12 was developed and investigated. This method was successfully demonstrated to synthesize high quality crystals of PCN-12 and removed the necessity of tedious synthesis procedure and potentially reduce the workload and financial cost of producing the material for potential applications. The detailed studies provided insights on importance of synthesizing high-quality crystals to accurately assess the porosity and hydrogen storage performance of a MOF. Furthermore, PCN-12 was found to be a promising material with high hydrogen storage capacity at 77 K.

In the second project, a synthesis of MOF with tetrazolate linker based on PCN-12 structure to provide a material with higher hydrogen storage capacity was attempted. Synthesis of the tetrazole linker was achieved and characterized using nuclear magnetic resonance and mass spectroscopy. However, detailed screening studies have failed to yield crystalline structures which is fundamental to study MOFs due to their crystalline nature, therefore, the possible structures could not be studied by crystallography or gas sorption studies to investigate its performance as a potential hydrogen storage material as intended. More screening studies using methods like as high-throughput synthesis could potentially be applied to yield the desired crystalline structures.

REFERENCES

1. Schlapbach, L.; Züttel, A., Hydrogen-storage materials for mobile applications. *Nature* **2001,** *414* (6861), 353-358.

2. Orimo, S.-i.; Nakamori, Y.; Eliseo, J. R.; Züttel, A.; Jensen, C. M., Complex Hydrides for Hydrogen Storage. *Chemical Reviews* **2007,** *107* (10), 4111-4132.

3. Langmi, H. W.; Walton, A.; Al-Mamouri, M. M.; Johnson, S. R.; Book, D.; Speight, J. D.; Edwards, P. P.; Gameson, I.; Anderson, P. A.; Harris, I. R., Hydrogen adsorption in zeolites A, X, Y and RHO. *Journal of Alloys and Compounds* **2003,** *356-357*, 710-715.

4. von Helmolt, R.; Eberle, U., Fuel cell vehicles: Status 2007. *Journal of Power Sources* **2007,** *165* (2), 833-843.

5. Furukawa, H.; Ko, N.; Go, Y. B.; Aratani, N.; Choi, S. B.; Choi, E.; Yazaydin, A. Ö.; Snurr, R. Q.; O'Keeffe, M.; Kim, J.; Yaghi, O. M., Ultrahigh Porosity in Metal-Organic Frameworks. *Science* **2010,** *329* (5990), 424-428.

6. Stock, N.; Biswas, S., Synthesis of Metal-Organic Frameworks (MOFs): Routes to Various MOF Topologies, Morphologies, and Composites. *Chemical Reviews* **2012,** *112* (2), 933-969.

7. Feng, D.; Wang, K.; Wei, Z.; Chen, Y.-P.; Simon, C. M.; Arvapally, R. K.; Martin, R. L.; Bosch, M.; Liu, T.-F.; Fordham, S.; Yuan, D.; Omary, M. A.; Haranczyk, M.; Smit, B.; Zhou, H.-C., Kinetically tuned dimensional augmentation as a versatile synthetic route towards robust metal–organic frameworks. *Nature Communications* **2014,** *5*, 5723.

8. Farha, O. K.; Özgür Yazaydın, A.; Eryazici, I.; Malliakas, C. D.; Hauser, B. G.; Kanatzidis, M. G.; Nguyen, S. T.; Snurr, R. Q.; Hupp, J. T., De novo synthesis of a metal–organic framework material featuring ultrahigh surface area and gas storage capacities. *Nature Chemistry* **2010,** *2*, 944.

9. Kaye, S. S.; Dailly, A.; Yaghi, O. M.; Long, J. R., Impact of Preparation and Handling on the Hydrogen Storage Properties of Zn4O(1,4-benzenedicarboxylate)3 (MOF-5). *Journal of the American Chemical Society* **2007,** *129* (46), 14176-14177.

10. Salem, M. M. K.; Braeuer, P.; Szombathely, M. v.; Heuchel, M.; Harting, P.; Quitzsch, K.; Jaroniec, M., Thermodynamics of High-Pressure Adsorption of Argon, Nitrogen, and Methane on Microporous Adsorbents. *Langmuir* **1998,** *14* (12), 3376-3389.

11. Mason, J. A.; Veenstra, M.; Long, J. R., Evaluating metal–organic frameworks for natural gas storage. *Chemical Science* **2014,** *5* (1), 32-51.

12. Panella, B.; Hirscher, M.; Roth, S., Hydrogen adsorption in different carbon nanostructures. *Carbon* **2005,** *43* (10), 2209-2214.

13. Suh, M. P.; Park, H. J.; Prasad, T. K.; Lim, D.-W., Hydrogen Storage in Metal–Organic Frameworks. *Chemical Reviews* **2012,** *112* (2), 782-835.

14. Wang, X.-S.; Ma, S.; Rauch, K.; Simmons, J. M.; Yuan, D.; Wang, X.; Yildirim, T.; Cole, W. C.; López, J. J.; Meijere, A. d.; Zhou, H.-C., Metal−Organic Frameworks Based on Double-Bond-Coupled Di-Isophthalate Linkers with High Hydrogen and Methane Uptakes. *Chemistry of Materials* **2008,** *20* (9), 3145-3152.

15. Lin, X.; Telepeni, I.; Blake, A. J.; Dailly, A.; Brown, C. M.; Simmons, J. M.; Zoppi, M.; Walker, G. S.; Thomas, K. M.; Mays, T. J.; Hubberstey, P.; Champness, N. R.; Schröder, M., High Capacity Hydrogen Adsorption in Cu(II) Tetracarboxylate Framework Materials: The Role of Pore Size, Ligand Functionalization, and Exposed Metal Sites. *Journal of the American Chemical Society* **2009,** *131* (6), 2159-2171.

16. Ma, S.; Simmons, J. M.; Sun, D.; Yuan, D.; Zhou, H.-C., Porous Metal-Organic Frameworks Based on an Anthracene Derivative: Syntheses, Structure Analysis, and Hydrogen Sorption Studies. *Inorganic Chemistry* **2009,** *48* (12), 5263-5268.

17. Goldsmith, J.; Wong-Foy, A. G.; Cafarella, M. J.; Siegel, D. J., Theoretical Limits of Hydrogen Storage in Metal–Organic Frameworks: Opportunities and Trade-Offs. *Chemistry of Materials* **2013,** *25* (16), 3373-3382.

18. Jia, Z.; Li, H.; Yu, Z.; Wang, P.; Fan, X., Densification of MOF-5 synthesized at ambient temperature for methane adsorption. *Materials Letters* **2011,** *65* (15), 2445-2447.

19. Zacharia, R.; Cossement, D.; Lafi, L.; Chahine, R., Volumetric hydrogen sorption capacity of monoliths prepared by mechanical densification of MOF-177. *Journal of Materials Chemistry* **2010,** *20* (11), 2145-2151.

20. Tian, T.; Zeng, Z.; Vulpe, D.; Casco, M. E.; Divitini, G.; Midgley, P. A.; Silvestre-Albero, J.; Tan, J.-C.; Moghadam, P. Z.; Fairen-Jimenez, D., A sol–gel monolithic metal–organic framework with enhanced methane uptake. *Nature Materials* **2017,** *17*, 174.

21. Bhatia, S. K.; Myers, A. L., Optimum Conditions for Adsorptive Storage. *Langmuir* **2006,** *22* (4), 1688-1700.

22. Frost, H.; Snurr, R. Q., Design Requirements for Metal-Organic Frameworks as Hydrogen Storage Materials. *The Journal of Physical Chemistry C* **2007,** *111* (50), 18794-18803.

23. Sircar, S., Estimation of isosteric heats of adsorption of single gas and multicomponent gas mixtures. *Industrial & Engineering Chemistry Research* **1992,** *31* (7), 1813-1819.

24. Wu, H.; Zhou, W.; Yildirim, T., High-Capacity Methane Storage in Metal−Organic Frameworks M2(dhtp): The Important Role of Open Metal Sites. *Journal of the American Chemical Society* **2009,** *131* (13), 4995-5000.

25. Zhou, W.; Wu, H.; Yildirim, T., Enhanced H2 Adsorption in Isostructural Metal−Organic Frameworks with Open Metal Sites: Strong Dependence of the Binding Strength on Metal Ions. *Journal of the American Chemical Society* **2008,** *130* (46), 15268-15269.

26. Wang, X.-S.; Ma, S.; Forster, P. M.; Yuan, D.; Eckert, J.; López, J. J.; Murphy, B. J.; Parise, J. B.; Zhou, H.-C., Enhancing H2 Uptake by "Close-Packing" Alignment of Open Copper Sites in Metal–Organic Frameworks. *Angewandte Chemie International Edition* **2008,** *47* (38), 7263-7266.

27. Cavka, J. H.; Jakobsen, S.; Olsbye, U.; Guillou, N.; Lamberti, C.; Bordiga, S.; Lillerud, K. P., A New Zirconium Inorganic Building Brick Forming Metal Organic

Frameworks with Exceptional Stability. *Journal of the American Chemical Society* **2008,** *130* (42), 13850-13851.

28. Blanc, J. R. L.; Sharp, D. B.; Murray, J. G., Di- and Tetracarboxydiphenylmethanes and Derivatives. *The Journal of Organic Chemistry* **1961,** *26* (11), 4731-4733.

29. Yan, Y.; da Silva, I.; Blake, A.; Dailly, A.; Manuel, P.; Yang, S.; Schröder, M., *High Volumetric Hydrogen Adsorption in a Porous Anthracene-Decorated Metal–Organic Framework*. 2018; Vol. 57.

30. Yan, Y.; Suyetin, M.; Bichoutskaia, E.; Blake, A. J.; Allan, D. R.; Barnett, S. A.; Schröder, M., Modulating the packing of [Cu24(isophthalate)24] cuboctahedra in a triazole-containing metal–organic polyhedral framework. *Chemical Science* **2013,** *4* (4), 1731-1736.

31. Wenzel, S. E.; Fischer, M.; Hoffmann, F.; Fröba, M., A new series of isoreticular copper-based metal–organic frameworks containing non-linear linkers with different group 14 central atoms. *Journal of Materials Chemistry* **2012,** *22* (20), 10294-10302.

32. Feng, G.; Peng, Y.; Liu, W.; Chang, F.; Dai, Y.; Huang, W., Polar Ketone-Functionalized Metal–Organic Framework Showing a High CO2 Adsorption Performance. *Inorganic Chemistry* **2017,** *56* (5), 2363-2366.

33. Rajca, A.; Padmakumar, R.; Smithhisler, D. J.; Desai, S. R.; Ross, C. R.; Stezowski, J. J., Synthesis of [1.1.1.1]Metacyclophane Macrocycle. *J Org Chem* **1994,** *59* (25), 7701-7703.

34. Zanon, J.; Klapars, A.; Buchwald, S. L., Copper-Catalyzed Domino Halide Exchange-Cyanation of Aryl Bromides. *Journal of the American Chemical Society* **2003,** *125* (10), 2890-2891.

35. Akhlaghinia, B.; Rezazadeh, S., A novel approach for the synthesis of 5-substituted-1H-tetrazoles. *Journal of the Brazilian Chemical Society* **2012,** *23,* 2197-2203.

36. Dincă, M.; Dailly, A.; Long, J. R., Structure and Charge Control in Metal–Organic Frameworks Based on the Tetrahedral Ligand Tetrakis(4-tetrazolylphenyl)methane. *Chemistry – A European Journal* **2008,** *14* (33), 10280-10285.